RESEARCH ARTICLE

RNA-mediated ribonucleoprotein assembly controls TDP-43 nuclear retention

Patricia M. dos Passos[1], **Erandika H. Hemamali**[1], **Lohany D. Mamede**[1], **Lindsey R. Hayes**[2], **Yuna M. Ayala**[1]*

1 Edward Doisy Department of Biochemistry and Molecular Biology, Saint Louis University School of Medicine, St. Louis, Missouri, United States of America, 2 Department of Neurology, Johns Hopkins University School of Medicine, Baltimore, Maryland, United States of America

* yuna.ayala@health.slu.edu

Abstract

TDP-43 is an essential RNA-binding protein strongly implicated in the pathogenesis of neurodegenerative disorders characterized by cytoplasmic aggregates and loss of nuclear TDP-43. The protein shuttles between nucleus and cytoplasm, yet maintaining predominantly nuclear TDP-43 localization is important for TDP-43 function and for inhibiting cytoplasmic aggregation. We previously demonstrated that specific RNA binding mediates TDP-43 self-assembly and biomolecular condensation, requiring multivalent interactions via N- and C-terminal domains. Here, we show that these complexes play a key role in TDP-43 nuclear retention. TDP-43 forms macromolecular complexes with a wide range of size distribution in cells and we find that defects in RNA binding or inter-domain interactions, including phase separation, impair the assembly of the largest species. Our findings suggest that recruitment into these macromolecular complexes prevents cytoplasmic egress of TDP-43 in a size-dependent manner. Our observations uncover fundamental mechanisms controlling TDP-43 cellular homeostasis, whereby regulation of RNA-mediated self-assembly modulates TDP-43 nucleocytoplasmic distribution. Moreover, these findings highlight pathways that may be implicated in TDP-43 proteinopathies and identify potential therapeutic targets.

Introduction

TDP-43 (TAR DNA-binding protein), a highly conserved and essential RNA-binding protein in multicellular eukaryotes, is central in the pathogenesis of neurodegenerative disorders. Accumulation of TDP-43 aggregates and loss of nuclear protein localization are hallmark features of almost all amyotrophic lateral sclerosis (ALS) and approximately 50% of frontotemporal dementia (FTD) patients [1–3]. In addition, TDP-43 pathology is a signature feature of an Alzheimer's disease (AD)-related dementia affecting the oldest population, termed limbic-predominant age-related TDP-43 encephalopathy (LATE) [4]. The majority of TDP-43 inclusions is observed in the cytoplasm and often corresponds to loss of nuclear localization. Structural defects in the nuclear pore complex linked to ALS and FTD promote TDP-43 cytoplasmic mislocalization, suggesting that aberrant nucleocytoplasmic transport impacts TDP-43 homeostasis in disease [5]. Aberrant accumulation of cytoplasmic TDP-43 is linked to

Abbreviations: AD, Alzheimer's disease; ALS, amyotrophic lateral sclerosis; CR, conserved region; CTD, C-terminal domain; DMEM, Dulbecco's Modified Eagle's Medium; FBS, fetal bovine serum; FTD, frontotemporal dementia; HA, hemagglutinin; hnRNP, heterogeneous ribonucleoprotein; LATE, limbic-predominant age-related TDP-43 encephalopathy; LLPS, liquid–liquid phase separation; NLS, nuclear localization signal; NTD, N-terminal domain; PBS, phosphate-buffered saline; RNP, ribonucleoprotein; RRM, RNA recognition motif; SEC, size exclusion chromatography; WT, wild type.

increased protein aggregation and is thought to promote depletion of the nuclear pool of functional TDP-43 in affected cells [6–8]. Maharana and colleagues proposed that the relatively lower levels of RNA in the cytoplasm are a major factor contributing to aggregation of TDP-43 and other RNA-binding proteins in this compartment [9]. While in the nucleus, RNA binding may prevent TDP-43 misfolding despite the higher concentration of TDP-43. Data from our group and others support this model by showing that specific RNA binding decreases TDP-43 aggregation and promotes liquid properties during phase separation [7,10]. Therefore, defects in TDP-43 nuclear retention may strongly contribute to pathogenesis by increasing the cytoplasmic accumulation of the protein. At the same time, loss of nuclear localization decreases TDP-43 nuclear functions, such as control of gene expression [11–14], as detected in neurons extracted from ALS/FTD patient brain devoid of nuclear TDP-43 [15]. Indeed, dysregulation of TDP-43 targets is observed in patients [16–19], supporting the idea that loss of nuclear localization strongly impairs physiological TDP-43 function contributing to disease.

TDP-43 shuttles continuously between the nuclear and cytoplasmic compartments, but is normally predominantly nuclear as shown by fractionation experiments and cell imaging [20]. TDP-43 undergoes active nuclear import mediated by a basic bipartite nuclear localization signal (NLS) (**Fig 1A**) and binding to importins α/β (karyopherins α/β) [6,21]. In addition, alternative mechanisms may also actively or passively promote nuclear entry [22–24]. A nuclear export signal was previously proposed to interact with exportin 1 (XPO/CRM1) [6]; however, multiple lines of evidence indicate that TDP-43 passively exits the nucleus in a size-dependent manner [23–26] through nuclear pore channels, which increasingly exclude cargoes above 30 to 60 kDa in size [22,27]. Recent findings suggest that binding to nuclear RNAs restricts TDP-43 availability for passive exit through nuclear pore channels [26]. Thus, TDP-43 incorporation into high molecular weight nuclear ribonucleoproteins (RNPs) may be a key mechanism promoting TDP-43 nuclear accumulation.

TDP-43 is a heterogeneous ribonucleoprotein (hnRNP) composed of multiple independently folded domains and a mostly disordered C-terminal region (**Fig 1A**). The N-terminal domain (NTD) resembles ubiquitin-like Dishevelled/Axin (DIX) domains and forms dimers/oligomers through head-to-tail interactions [28,29]. Two tandem RNA recognition motifs (RRMs) bind RNA with strong preference for GU-rich sequences, which are recognized with affinity in the low nanomolar range [30,31]. The C-terminal domain (CTD) is a low complexity sequence region also referred to as prion-like domain. The isolated CTD undergoes liquid–liquid phase separation (LLPS) in vitro [32] and is believed to largely contribute to TDP-43 condensation in cells [33]. In particular, an evolutionarily conserved region (CR, a.a. 320–343) in the CTD that forms a partial α-helical structure [34] mediates homotypic assembly and LLPS in vitro and in cells [32,33]. This process of biomolecular condensation is increasingly believed to mediate the formation of protein and RNA-rich assemblies or RNP complexes [35,36]. In cells, TDP-43 forms and is recruited to RNPs, such as Cajal bodies, and stress granules [37,38]. We recently showed that RNA binding to extended GU-rich sequences promotes TDP-43 biomolecular condensation in vitro and in mammalian cell lysate reconstitution assays [10]. Consistent with the strong contribution of biopolymers and multivalent interactions to the formation of biomolecular condensates [39], we found that RNA-mediated TDP-43 condensates require NTD and CTD-mediated interactions, as shown in our model (**Fig 1A**). These TDP-43 assemblies are necessary for the regulation of RNA processing, as shown in the case of TDP-43 autoregulation [40]. This notion is supported by Hallegger and colleagues, who also showed that TDP-43 phase separation determines the recruitment to RNA transcripts with specific sequence composition [41].

Here, we investigated the role of RNA-mediated TDP-43 self-assembly through oligomerization and phase separation in regulating cellular distribution and examined the relative
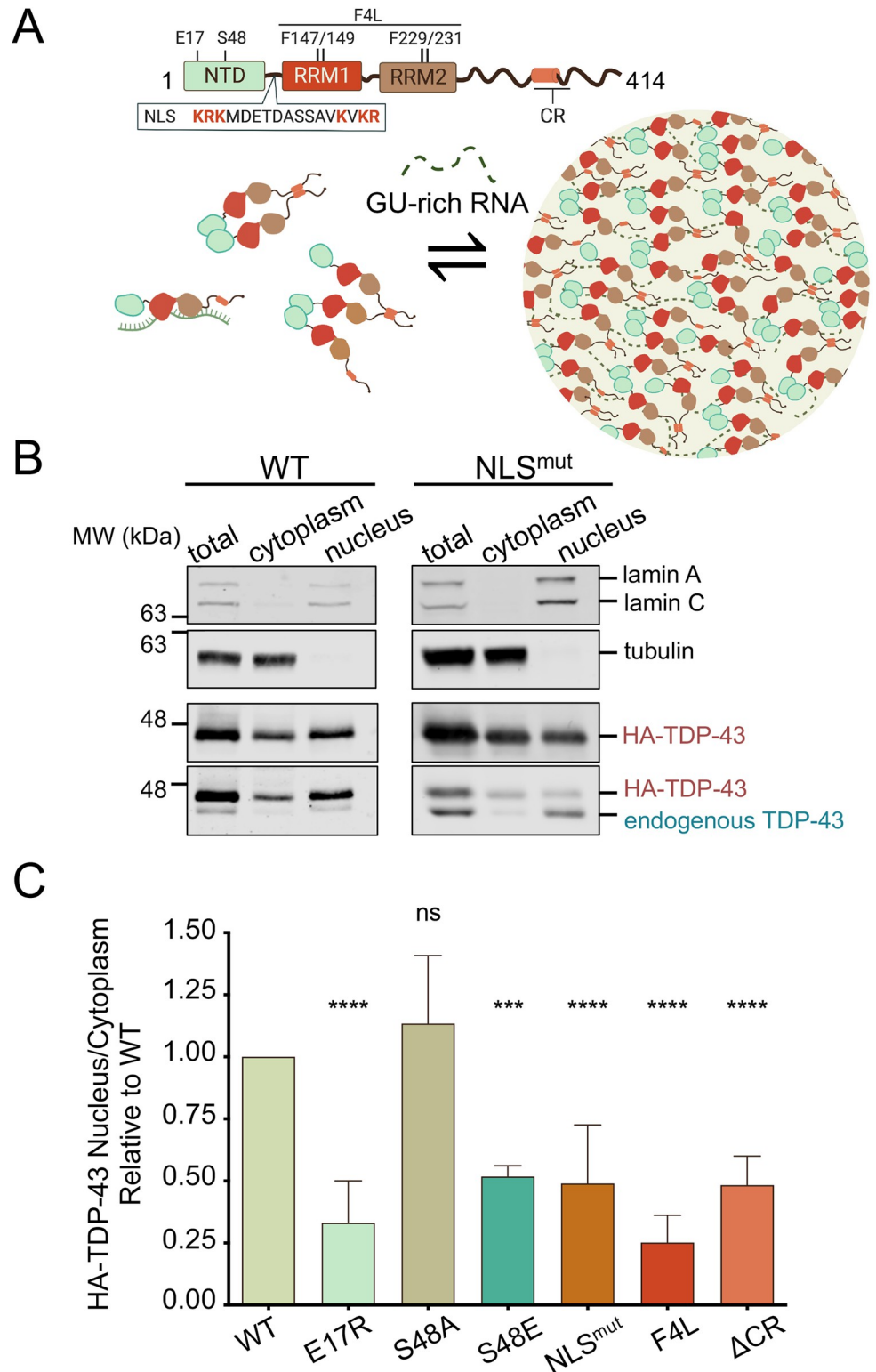
Fig 1. Defects in RNA-mediated TDP-43 self-assembly decrease nuclear localization. (A) TDP-43 domain organization and model of RNA-mediated TDP-43 self-assembly involving multivalent interactions through the NTD oligomerization and C-terminal assembly. Mutations in the NTD, RRMs, and deletion of the conserved α-helical region (ΔCR) in the C-tail (a.a. 316–343) are highlighted. The basic residues (red) in the NLS were substituted to generate NLS[mut], used as control. (B) Immunoblot of total, cytoplasmic and nuclear fractions of HEK293[HA-TDP-43]

contribution of each of these interactions to the native molecular weight of these RNP complexes. We demonstrate that RNA binding and multi-domain interactions form large macromolecular assemblies that act in combination to maintain TDP-43 nuclear localization by preventing nuclear exit. Our work highlights important mechanisms regulating TDP-43 cellular homeostasis by showing that these macromolecular complexes increase nuclear retention in a size-dependent manner and are tightly regulated by RNA-mediated phase separation.

Results

TDP-43 multivalent interactions are necessary for TDP-43 nuclear localization

Mounting evidence, including our previous studies, indicate that RNA binding increases nuclear TDP-43 localization [20,26]. In addition, our recent work showed that RNA binding, in the presence of multivalent interactions, induces biomolecular condensation or LLPS [10]. We therefore asked whether these RNA-bound complexes play a role in TDP-43 nuclear retention by investigating how disruptions in their assembly alter cellular distribution. We analyzed site-specific mutations in different TDP-43 domains previously established to impair self-assembly (**Fig 1A**), using an engineered human cell line stably expressing a single copy of hemagglutinin (HA)-tagged wild-type (WT) or TDP-43 variants upon induction with tetracycline (Tet) [40]. This collection of human embryonic kidney isogenic cell lines (HEK293$^{\text{HA-TDP-43}}$) expressed WT and mutant TDP-43 at close to endogenous levels. The small HA tag was specifically used to minimize size-dependent disruption of cellular trafficking. To measure nuclear-cytoplasmic distribution, nucleus and cytoplasm were biochemically separated after 72 h of transgene induction. TDP-43 levels in nuclear and cytoplasmic fractions were measured by immunoblotting (**Figs 1B, S1A and S1B**) and expressed as the nuclear-cytoplasmic ratio (N/C) (**Fig 1C**). Lamin A/C and tubulin were used to normalize samples and to determine the integrity of nuclear and cytoplasmic fractions for each experiment. The same assays were previously utilized to show that TDP-43 predominantly localizes in the nucleus [20]. The anti-TDP-43 antibody detected low levels of endogenous TDP-43 upon HA-WT TDP-43 expression (**Fig 1B**), which is consistent with TDP-43 autoregulatory function [12,42]. A mutant disrupting the nuclear localization signal (NLS$^{\text{mut}}$, K^{82}RK^{84}/K^{95}VKR^{98} to A^{82}AA^{84}/A^{95}VAA^{98}) [6] was used as a control (**Fig 1A**). Each independent replicate was performed in parallel with WT-expressing cells, and the N/C was calculated relative to WT (**Fig 1C**). As expected, NLS$^{\text{mut}}$ levels increased in the cytoplasm, resulting in a 50% reduction in N/C, relative to WT. The immunoblot also showed loss of autoregulation as seen by the higher levels of endogenous TDP-43 in these cells compared to WT (**Fig 1B**). Endogenous TDP-43 nuclear-cytoplasmic distribution in NLS$^{\text{mut}}$-expressing cells was not affected by the presence of the mutant copy. In agreement with our previous results [20,26], nuclear retention was reduced by mutations in the RRMs that greatly impair specific RNA-binding affinity F147/149/229/231L (F4L) [10,43]. Next, we probed the role of NTD-driven oligomerization by disrupting interactions previously shown to be important for self-assembly [29]. The E17R substitution is sufficient to inhibit oligomerization [44] and impair RNA-driven LLPS [40]. We found that E17R significantly

reduced N/C by approximately 70%, relative to WT. Notably, this effect was even more pronounced than loss of the nuclear localization signal (NLS[mut]). The interaction between Glu17 and Ser48 from 2 independent NTDs is required for oligomerization [29]. Ser48 is subject to phosphorylation [44–46] and this is predicted to inhibit oligomerization as observed by the decrease in TDP-43 dimerization and LLPS in the presence of the phosphomimetic S48E substitution [44]. Consistent with the effect of E17R, we observed that S48E significantly reduced TDP-43 N/C by approximately 50% compared to WT. In contrast, the phospho-null mutant S48A, used as control, showed a moderate yet not significant increase in N/C relative to WT. Importantly, these results suggest that phosphorylation at Ser48 may regulate TDP-43 nuclear localization. We also found that deletion of the conserved region (ΔCR) in the CTD decreased the relative N/C by approximately 50%. To determine whether the differences observed were caused by changes in HA-TDP-43 protein expression, we measured the protein levels of across the WT and mutant isogenic cell lines. Our results showed no significant differences in mutant HA-TDP-43 levels in the total cell lysate, relative to WT (**S1C Fig**). Altogether, our observations suggest that RNA-dependent multivalent interactions through the NTD and CR at the C-terminus strongly promote TDP-43 nuclear localization. It is important to note that we observed greater endogenous TDP-43 expression in E17R, S48E, and F4L mutant cell lines, compared to WT. These findings were anticipated because TDP-43 autoregulation requires RNA binding and NTD-mediated oligomerization [40,42]. ΔCR would be similarly affected as the CR and condensate formation also contribute to autoregulation [40,41]. Thus, it is possible that increased endogenous TDP-43 levels contribute to the altered nuclear-cytoplasmic distribution of the mutants by competing for RNA binding or oligomerization. Further studies should explore this possibility.

To distinguish whether enhanced cytoplasmic localization of TDP-43 mutants (**Fig 1C**) was caused by defects in nuclear import, or increased nuclear efflux, we performed heterokaryon assays using WT and mutant HEK293[HA-TDP-43] cells. HEK293[HA-TDP-43] cells were fused with NIH3T3 mouse cells resulting in multinucleated cells (**Fig 2A**). Within 1 h of outer membrane fusion, WT HA-TDP-43 was observed in HEK293 nuclei (donor) as well as in mouse nuclei (acceptor) of heterokaryon cells, consistent with our previous findings [20] (**Fig 2B**). Mutants E17R, F4L, and ΔCR were also present in acceptor nuclei, indicating that the mutations did not impair nuclear import. Interestingly, we observed that at this time point WT TDP-43 levels in the donor nuclei remained greater compared to the acceptor, based on the fluorescence signal. In contrast, E17R, F4L, and ΔCR showed similar levels of HA-TDP-43 fluorescence in donor and acceptor nuclei. To further investigate these differences, we quantified the fluorescence ratio of donor versus acceptor nuclei (**Fig 2C**). WT TDP-43 donor to acceptor ratio was approximately 1.5, suggesting that at 1 h post heterokaryon formation, TDP-43 exits donor nuclei and is imported into the acceptor, but that a significant amount of protein, 50% more, is retained in donor nuclei. The mutants, in contrast, showed significant reductions of donor to acceptor ratio (approximately 50% to 25%), relative to WT. These results indicate that the increased cytoplasmic levels of E17R, F4L, and ΔCR, shown in **Fig 1**, are not the result of impaired nuclear import. Rather, disruption of TDP-43 self-assembly through the NTD and CR as well as RNA binding deficiency increase the rate of TDP-43 egress from the nucleus.

RNA binding and multi-domain TDP-43 interactions prevent nuclear exit synergistically

To define the relative contribution of NTD, CR-driven assembly, and RNA binding to TDP-43 nuclear retention, we investigated the role of RNA on the localization of NTD and ΔCR mutants. For these experiments, we measured nuclear and cytoplasmic TDP-43 levels in
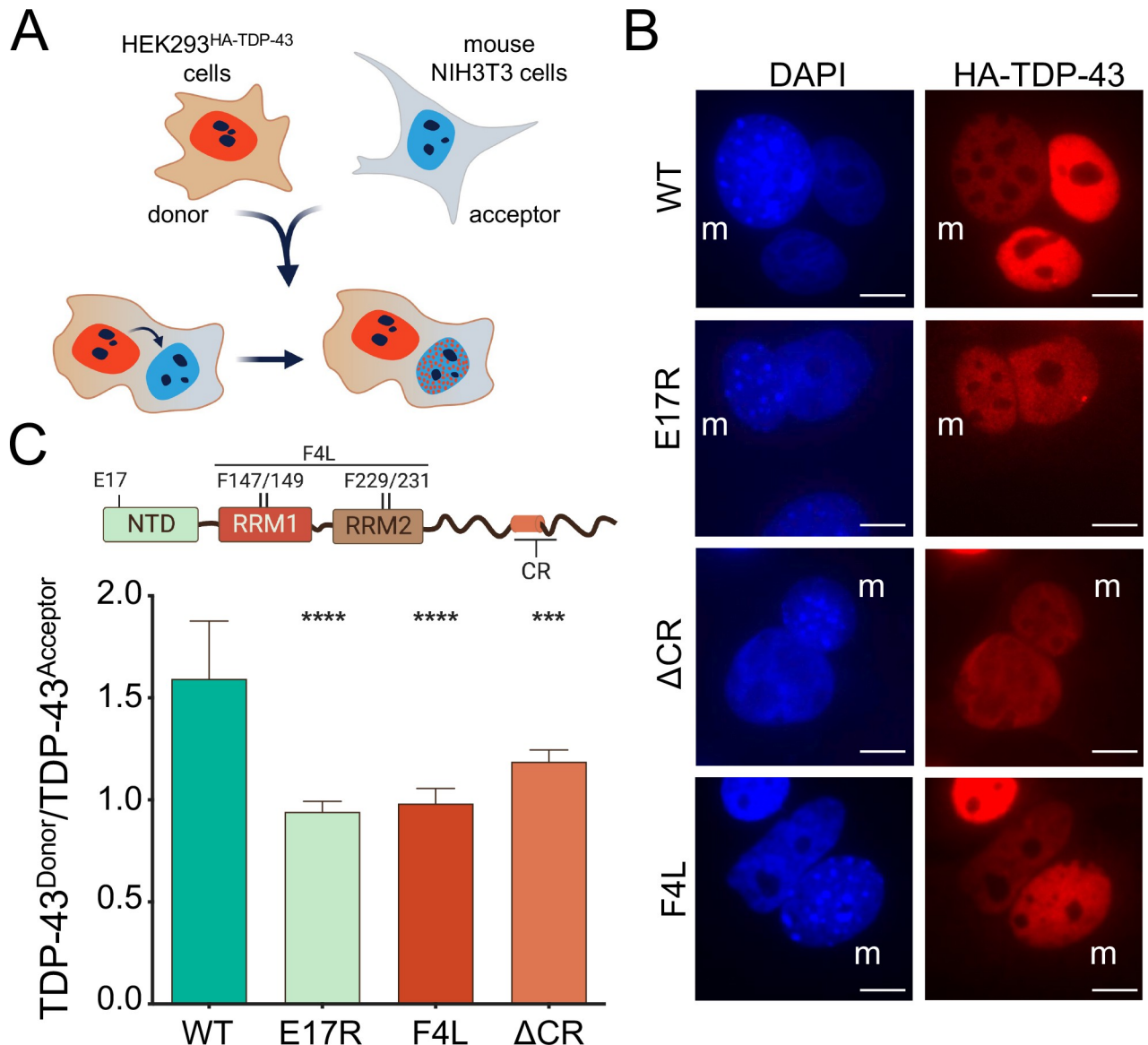
Fig 2. Disruption of RNA binding or TDP-43 self-assembly accelerates TDP-43 nuclear efflux. (A) Heterokaryon assays in which HEK293[HA-TDP-43] cells are fused to mouse NIH3T3 cells. HEK293[HA-TDP-43] nuclei (donor) and HA-TDP-43 signal are depicted in red, mouse NIH3T3 nuclei (acceptor) in blue. **(B)** Immunofluorescence of heterokaryons highlighting mouse nuclei (m). Scale bar, 10 μm. **(C)** Quantified HA-TDP-43 signal ratio of HEK293[HA-TDP-43] (donor) to mouse (acceptor) nuclei of heterokaryons. Mean ± SD shown for 7 independent replicates, 50 or more heterokaryons were quantified, source data can be found in S1 Data, ***$p < 0.001$, ****$p < 0.0001$, one-way ANOVA with Tukey's test compared to WT. HA, hemagglutinin; WT, wild type.

https://doi.org/10.1371/journal.pbio.3002527.g002

HEK293[HA-TDP-43] cells using confocal high-content imaging [26]. In agreement with the biochemical fractionation assays, E17R, F4L, and ΔCR showed significant reductions of TDP-43 N/C, compared to WT (**Fig 3A**). F4L caused a significantly greater loss of nuclear localization relative to E17R and ΔCR, highlighting a central role of RNA binding in maintaining high nuclear TDP-43 concentration. Treatment with the pan-transcriptional inhibitor Actinomycin D (Act D) reduced WT nuclear localization (**Fig 3B**), as previously observed [20,26]. Similarly, the specific RNA polymerase II inhibitor NVP2 [47] decreased WT TDP-43 N/C by approximately 40%, indicating that the observed changes are specific to decreased transcription. We

found that Act D and NVP2 treatment significantly decreased E17R and ΔCR N/C by approximately 45% and 20%, respectively, compared to untreated control cells. In contrast, localization of F4L was unaffected, consistent with the idea that transcriptional inhibition alters TDP-43 localization by decreasing the abundance of nuclear pre-mRNAs available for TDP-43 to bind. We then transfected cells with increasing amounts of $(GU)_6$ RNA oligonucleotides carrying a phosphorothioate backbone and 2′-O-methyl modifications to prevent degradation by RNases (reviewed in [48]). The $(CA)_6$ RNA sequence which shows no significant TDP-43 binding [43] was used as nonspecific control. Efficient cellular uptake and nuclear import of these RNA molecules was previously quantified [26]. In agreement with Duan and colleagues, $(GU)_6$ RNA induced a dose-dependent efflux of WT TDP-43 to the cytoplasm (**Fig 3C**), while the nonspecific RNA did not have an effect. E17R and ΔCR mutant N/C was decreased by $(GU)_6$ in the same manner as WT, suggesting that increasing levels of GU-rich RNA further impair nuclear retention of TDP-43 mutants with defects in self-assembly. On the other hand, F4L nuclear-cytoplasmic distribution was insensitive to the presence of $(GU)_6$ RNA, as expected. Our results indicate that RNA binding, NTD oligomerization, and CR-mediated self-assembly together contribute to TDP-43 nuclear retention and that the sum of these interactions is required to prevent protein efflux to the cytoplasm.

TDP-43 condensate formation promotes nuclear retention

RNA-binding proteins, including TDP-43 and related ALS/FTD-associated proteins, undergo phase separation and condensate formation as purified components and in cells [49–52]. The conserved α-helical region within the CTD of TDP-43 is essential for promoting phase separation in the context of the isolated domain and full-length protein [32,41]. We showed that this region is also necessary to form RNA-mediated TDP-43 condensates [40]. To determine whether the decrease in nuclear localization upon deletion of the CR (**Fig 1C**) is caused by defects in phase separation, we measured TDP-43 nuclear-cytoplasmic distribution under conditions that inhibit condensate formation. 1,6-hexanediol (1,6-HD) is widely used to inhibit phase separation [53] and impairs droplet formation of purified TDP-43 [7,54]; 1,6-HD also decreases the formation of nuclear TDP-43 foci in cells [41], suggesting that it reduces TDP-43 RNP condensates. We treated cells with 5% 1,6-HD for 5 min and observed a 5-fold decrease in N/C of endogenous TDP-43, compared to non-treated control cells (**Fig 4A**). This result corresponded to a dramatic shift in TDP-43 localization from the nucleus to the cytoplasm as seen by fluorescence microscopy (**Fig 4B**). We considered that 1,6-HD may also disrupt the phenylalanine-glycine (FG) permeability barrier in the central channel of the nuclear pore complex [55]. This effect could also contribute to the increased nuclear efflux of TDP-43 upon 1,6-HD treatment. To test disruption of TDP-43 condensate formation more specifically, we introduced mutations in the CR to modulate phase separation by altering α-helix structural properties (**Fig 4C**) [32,41]. A326P, M337P, and the ALS-linked mutation M337V are helix breaking mutants that result in aberrant CTD self-assembly and impaired LLPS [10,32,40]. Moreover, these single-site substitutions closely resemble the inhibition properties of ΔCR on the formation of TDP-43-rich nuclear foci and phase separation-dependent RNA processing of TDP-43 targets in cells [41]. We found significant decrease in nuclear TDP-43 localization with each of these mutations (**Fig 4C**), consistent with the effect of 1,6 HD treatment and deletion of the entire CR in Fig 1C. Differences between WT and mutant condensate/foci formation in cells may be visualized by immunofluorescence microscopy, although TDP-43 nuclear structures are less well defined in HEK293 cells compared to other cell types (e.g., U2-OS, HeLa). WT TDP-43 formed distinct nuclear foci that colocalized with coilin, which is a marker of Cajal bodies, in agreement with its recruitment to condensates and
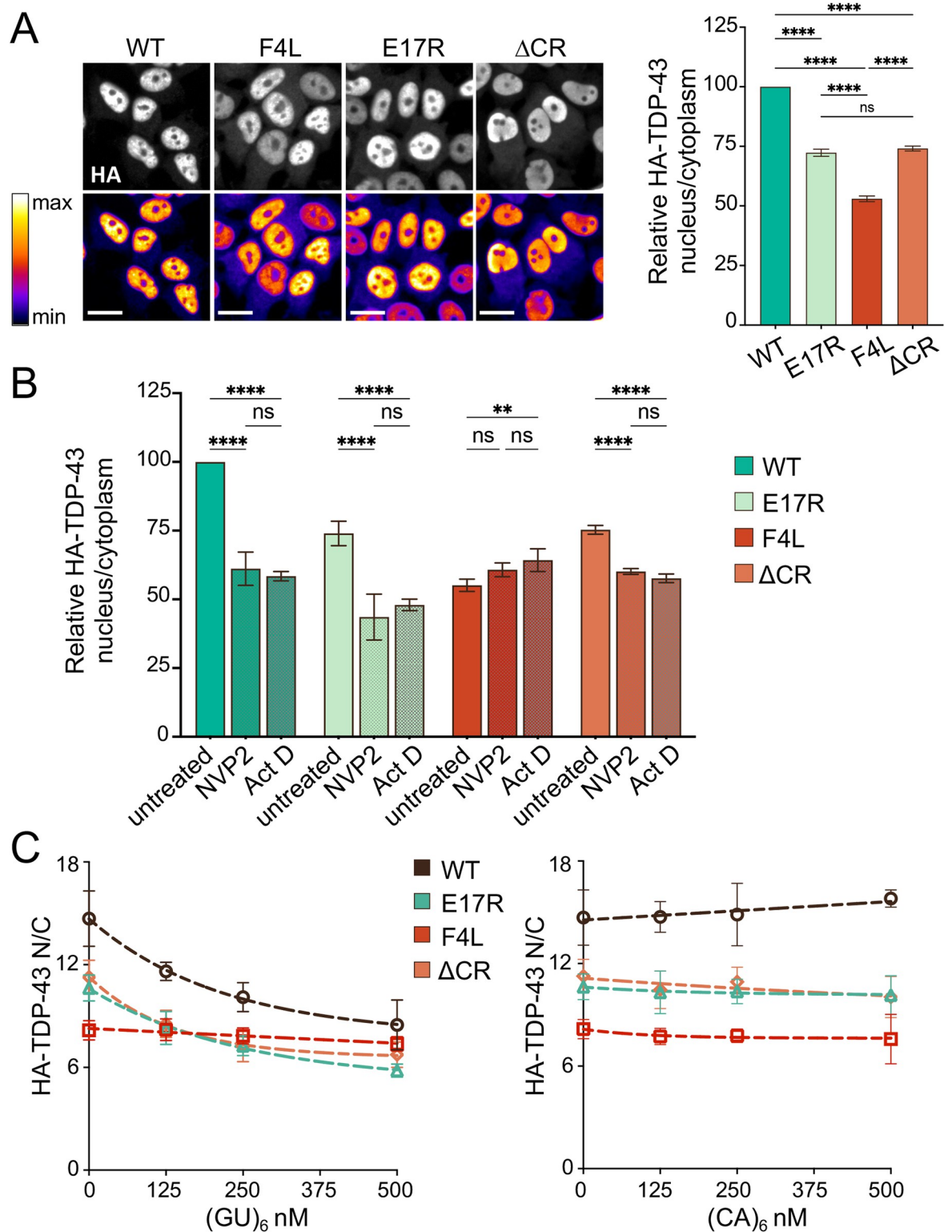
Fig 3. RNA binding and TDP-43 self-assembly exert independent and additive effects on TDP-43 nuclear localization. (A) HEK293[HA-TDP-43] cells expressing HA-tagged WT and mutant TDP-43 probed with HA antibody (top: immunofluorescence, bottom: pseudo-color look-up table). The intensity histogram for each image was independently maximized across the full range. Scale bar, 20 μm. Graph shows automated quantification of the TDP-43 nuclear/cytoplasmic ratio (N/C) at steady state, normalized to WT. Mean ± SD is shown for approximately 1,600 cells/well in 7 independent replicates. ns, not significant, ****$p < 0.0001$, one-way ANOVA with Tukey's

test. (B) HA-TDP-43 N/C quantified 2 h posttranscriptional blockade with actinomycin D (Act, 1 μm) or NVP2 (250 nM) vs. DMSO control, normalized to WT control cells. Mean ± SD is shown for approximately 1,700 cells in 4 independent replicates. ns, not significant, **$p < 0.01$, ****$p < 0.0001$, two-way ANOVA with Tukey's test. (C) HA-TDP-43 N/C quantified 5 h post-transfection with increasing concentrations of $(GU)_6$ or $(CA)_6$ oligonucleotides. Mean ± SD is shown for approximately 1,700 cells/well in 5 independent replicates. Source data can be found in S1 Data. HA, hemagglutinin; WT, wild type.

https://doi.org/10.1371/journal.pbio.3002527.g003

membraneless organelles (S3 Fig). Upon quantification, an average of 23+/−4% of nuclei showed 2 or more puncta in the case of WT TDP-43 cells. The phospho-null mutant S48A showed similar results. In contrast, mutations disrupting TDP-43 phase separation, especially in the CTD, showed a diffuse pattern in the nucleoplasm, suggesting impaired LLPS. The phosphomimetic mutation S48E and E17R which inhibit NTD-mediated oligomerization showed <1% nuclei with puncta. Similarly, we were unable to quantify a significant number of nuclei with foci in cell lines expressing the CTD mutants. This analysis was performed with 3 independent replicates counting at least 50 cells per group. Our results are consistent with the inability of the mutations to form condensates as shown by our previous work [10,40] and others [32,41,44,56]. Together, these data strongly suggest that nuclear condensate formation plays a key role in regulating nuclear-cytoplasmic TDP-43 trafficking by promoting nuclear localization.

We note that F4L cells were excluded from quantification as loss of RNA binding alters TDP-43 nuclear foci in a unique way. While F4L inhibits RNA-mediated condensate formation [10] and decreases nuclear retention (Figs 1C, 2C and 3A), this and similar mutations inhibiting RNA binding form abundant nuclear puncta that are smaller compared to WT TDP-43. This is observed in the absence of over expression. The mechanisms driving the biogenesis and the properties of RNA-deficient TDP-43 complexes in nuclei remain unknown and should be the focus of further investigation.

The size of RNA-bound TDP-43 macromolecular complexes controls nuclear retention

Previous evidence indicates that TDP-43 nuclear efflux is largely a passive, size dependent process, whereby larger fusion constructs reduce TDP-43 export [23,24]. TDP-43 forms complexes of a wide range of sizes in cells, from monomers to large higher-order complexes greater than 1.5 MDa, as measured by size exclusion chromatography (SEC) [57,58]. Based on these findings, we tested whether the contribution of TDP-43 RNA-mediated complexes to nuclear retention is size dependent, requiring the formation of large macromolecular complexes. We analyzed the size distribution of TDP-43 in HEK293^HA-TDP-43 cell lysates expressing WT and mutant TDP-43 using gel filtration chromatography. Of note, the use of these isogenic cell lines expressing TDP-43 variants at endogenous-like levels was designed to avoid unintended effects of TDP-43 overexpression. The relative HA-TDP-43 levels in each eluted fraction was analyzed by immunoblotting to compare the approximate size distribution of WT versus mutant TDP-43 assemblies (Figs 5A and S4). We observed a broad profile of WT TDP-43 distribution starting at the estimated 45 kDa fraction to 700 kDa, which is the upper detection limit of the SEC column. The highest level of detected WT protein eluted at approximately 115 kDa and this was set as 100% (Fig 5B). Disruption of NTD-mediated oligomerization, E17R, showed a shift to higher elution volume compared to WT, whereby the peak of highest concentration moved to smaller estimated molecular weight, between 45 and 72 kDa (Fig 5C). In addition, TDP-43 levels in the fractions corresponding to higher molecular weight complexes were markedly decreased compared to WT. These results are consistent with previous cross-linking assays indicating a loss of multimeric TDP-43 species in cells upon disruption of
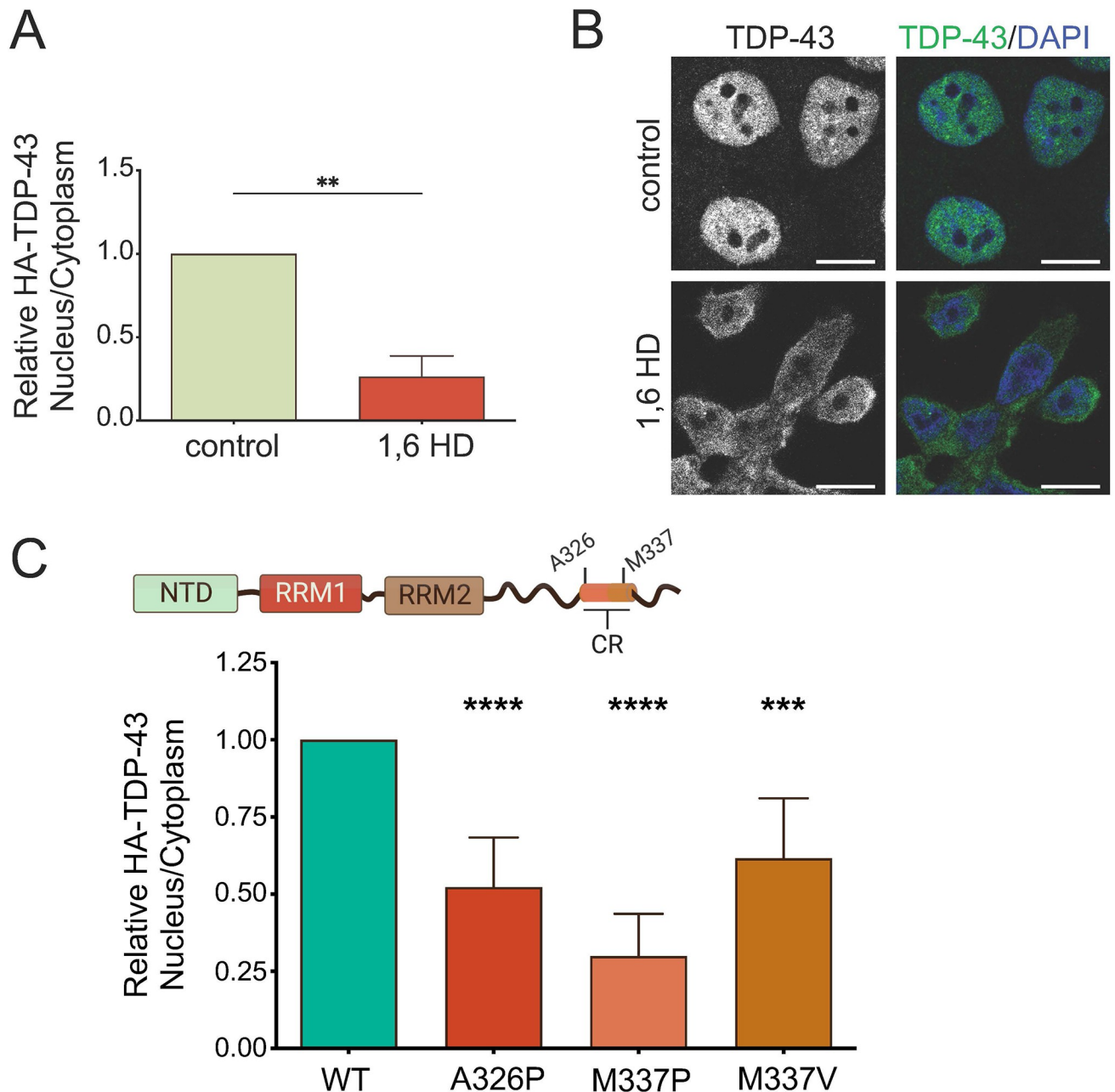
Fig 4. Inhibition of phase separation disrupts TDP-43 nuclear retention. (A) Relative nuclear to cytoplasmic signal ratio (N/C) of endogenous TDP-43 in HEK293 cells treated with 1,6 hexanediol (HD, 5% for 5 min) quantified from immunoblotting (S2A Fig), expressed relative to non-treated control. Mean ± SD is shown for 6 independent replicates. (B) Immunofluorescence of control and 1,6-HD-treated HEK293 cells, as seen by confocal microscopy. Polyclonal TDP-43 antibody was used to detect endogenous TDP-43 distribution. Scale bar, 10 μm. (C) HEK293[HA-TDP-43] cells expressing HA-tagged WT and A326P, M337P, and M337V mutants located in the conserved α-helical region (CR). Quantification of N/C of HA-TDP-43 relative to WT in each replicate from immunoblotting (S2B Fig). Mean ± SD is shown for 6 independent replicates. ***$p < 0.001$, ****$p < 0.0001$, one-way ANOVA with Tukey's test. Immunoblots and source data can be found in S2 Fig and in S1 Data, respectively. CR, conserved region; HA, hemagglutinin; WT, wild type.

https://doi.org/10.1371/journal.pbio.3002527.g004

NTD-mediated oligomerization [29]. Similar behavior was observed with the RNA-binding-deficient F4L mutant. The most abundant F4L fractions shifted to smaller estimated sizes compared to WT together with a dramatic sharpening of the elution profile. An even greater shift in size distribution was observed with ΔCR, showing an elution peak of estimated 45 kDa. In
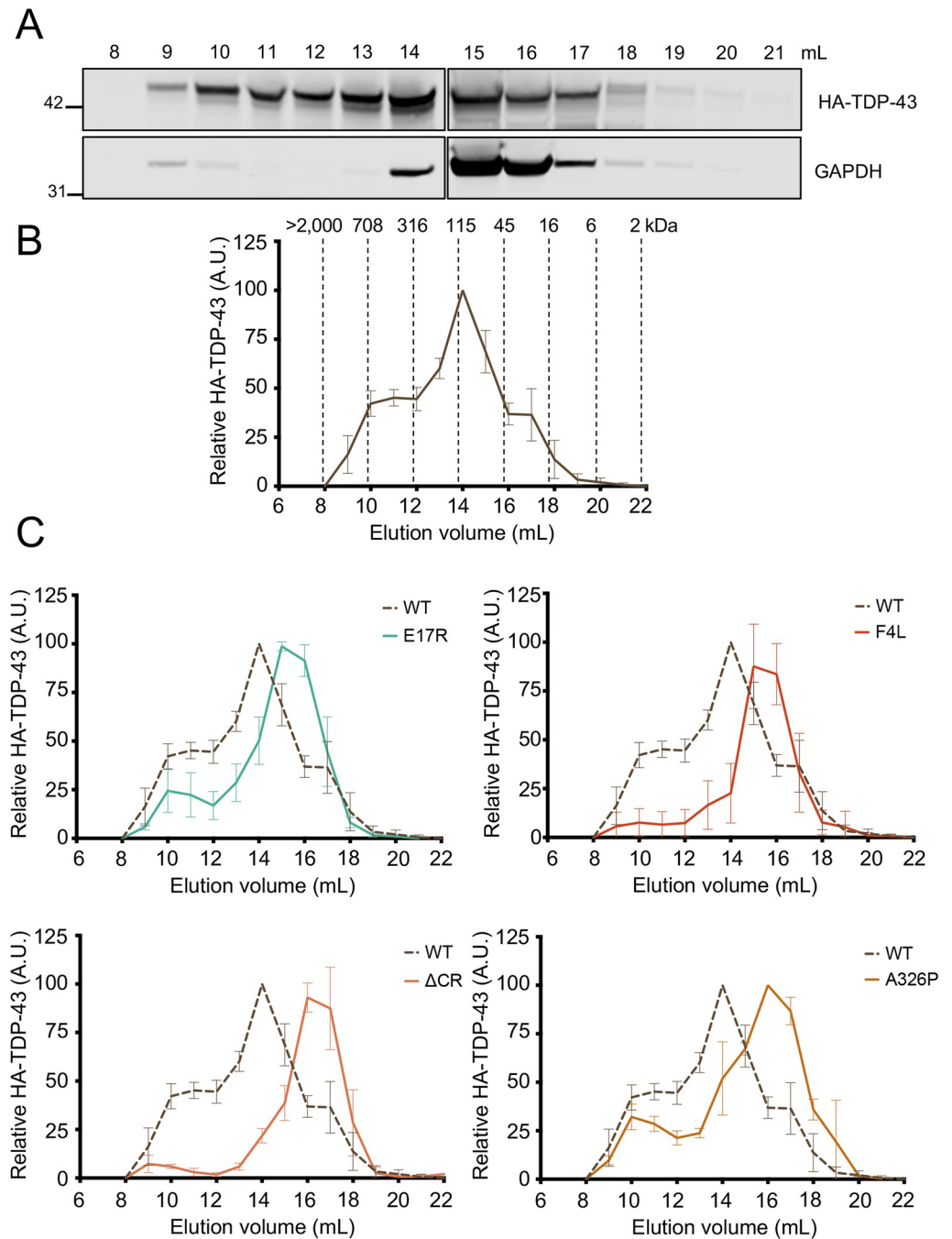
Fig 5. Disruption of RNA binding, NTD oligomerization, and phase separation inhibits large macromolecular TDP-43 complexes in cells. (A) Immunoblot detecting HA-TDP-43 levels in fractions eluted from gel filtration SEC of HEK293[HA-TDP-43] cell lysate. Membranes were probed with HA antibody and GAPDH as control. (B) WT HA-TDP-43 levels quantified in each elution fraction expressed as percent relative to the most abundant TDP-43 fraction. Mean ± SD is shown for 4 independent replicates. The estimated molecular weight is shown for each fraction based on calibration experiments. (C) Comparison of elution profiles for WT (dashed) vs. mutant (solid) TDP-43. Mean ± SD is shown for ≥3 independent replicates. Immunoblots and source data can be found in **S4 Fig** and S1 Data, respectively. HA, hemagglutinin; SEC, size exclusion chromatography; WT, wild type.

https://doi.org/10.1371/journal.pbio.3002527.g005

stark contrast with WT, little or no detection of ΔCR was observed above the estimated 115 kDa fraction. Based on the estimated size separation in our experiments, the altered behavior of ΔCR is unlikely to be caused by the 20 amino acid difference between this construct, WT and the other mutants analyzed here. To further test the role of CR-mediated assembly and LLPS on the size of TDP-43 complexes, we studied the effect of A326P. In agreement with ΔCR, A326P also reduced the size of the most abundant TDP-43 complexes, eluting at the estimated 45 kDa fraction. These results are consistent with an important role of CR-mediated homotypic assembly and LLPS in forming higher-order RNP bodies. Collectively, our SEC experiments provide biochemical evidence that disruption of NTD oligomerization, RNA binding, and phase separation decrease the size of TDP-43-rich complexes by impairing formation of the largest macromolecular species in cells. In addition, our data strongly suggest that the decreased ability to form these higher-order macromolecular assemblies reduces TDP-43 nuclear retention by increasing the population of protein freely diffusing to the cytoplasm.

Discussion

The normal distribution of TDP-43 between nuclear and cytoplasmic compartments, in which the protein is predominantly found in the nucleus, plays a central role in physiological function. Disruption of homeostasis is associated with pathogenesis in neurodegenerative disorders, wherein pathological decrease in nuclear TDP-43 and elevated protein levels in the cytoplasm are linked to TDP-43 loss of function and aggregation, respectively [1,2,15]. TDP-43 is recruited to RNA and protein-rich RNP complexes through RNA binding, TDP-43 self-assembly, and condensate formation/phase separation [59]. The mechanisms by which these complexes regulate TDP-43 function and homeostasis are only beginning to be explored. Recently, we showed that RNA-mediated TDP-43 phase separation depends on multivalent interactions involving NTD oligomerization and assembly through an α-helical conserved region at the C-terminus (CR) (**Fig 1A**) [10,40], which is essential for TDP-43 condensation in vitro and in cells [32,41,60]. Here, we find that disruption in any of the assembly points necessary to form RNA-mediated TDP-43 complexes is sufficient to markedly increase cytoplasmic localization. Thus, TDP-43 recruitment into RNP bodies plays a critical function in maintaining nuclear retention.

Based on emerging evidence, RNA binding plays a key role in TDP-43 molecular dynamics and proteostasis. We recently showed that specific RNA binding modulates TDP-43 phase separation properties [10] and that formation of these complexes is essential in regulating TDP-43 target expression, such as its own transcript during autoregulation [40,41]. The importance of RNA in TDP-43 nuclear localization was previously demonstrated with RNA binding-deficient mutants and by showing that inhibition of RNA transcription promotes cytoplasmic localization [20,26]. In addition, Duan and colleagues recently quantified the effect of TDP-43-RNA interactions in cells and showed that inhibition of splicing increases TDP-43 nuclear levels probably by increasing the retention of introns with TDP-43 recruitment sites [26]. In addition, small GU-rich RNA oligonucleotides, which bind TDP-43 with nanomolar affinity [30], promote the cytoplasmic egress of TDP-43 [26]. These data suggest that these RNA molecules promote the release of nuclear TDP-43 by competing with transcripts for TDP-43 binding. Here, we find that mutants deficient in NTD and CR-driven interactions are similarly affected by $(GU)_6$ RNA compared to WT (**Fig 3C**). Thus, our observations indicate that RNA binding, NTD and CR interactions contribute synergistically in maintaining nuclear localization. Importantly, we and others showed that specific RNA interactions prevent TDP-43 aggregation [7,61] and promote liquid-like behavior of TDP-43 condensates [10]. These results

collectively suggest that RNA binding plays multiple essential roles in maintaining TDP-43 function. Specific RNA binding increases nuclear TDP-43 retention by mediating the formation of RNP assemblies. In addition, RNA interactions increase solubility in the nucleus despite the higher protein concentration in this compartment. This idea is consistent with previous observations that solubility and liquid properties of the related protein FUS are maintained by the abundance of RNA in the nucleus [9].

Our data agree with recent work from the Polymenidou lab published while our manuscript was in preparation [62]. Using cell-based models, including human neurons, Pérez-Berlanga and colleagues show that NTD-mediated oligomerization and RNA binding act cooperatively to increase nuclear localization and that both interactions are important to prevent TDP-43 aggregation. Here, we extend beyond these findings by showing that condensate formation is required for the assembly of complexes that increase TDP-43 nuclear retention (**Fig 4**), highlighting the importance of multivalent interactions in TDP-43 function. In addition, our heterokaryon assays demonstrate that the defects in nuclear localization observed upon disruption of TDP-43 RNA binding, oligomerization, or phase separation are not caused by diminished nuclear import (**Fig 2**). Instead, our results suggest that disruption of these interactions accelerate protein efflux to the cytoplasm. Moreover, our SEC studies are the first to biochemically correlate the ability of TDP-43 to form RNA-bound condensates with the formation of large higher-order macromolecular complexes in cells (**Fig 5**). Based on our observations, we propose that TDP-43 nuclear retention is largely dependent on the formation of large RNP granules, reducing the population of smaller species available for passive export to the cytoplasm (**Fig 6**). These results are important because they support a size-dependent nuclear retention mechanism of RNA-bound TDP-43 condensates and illustrate multiple possible mechanisms to modulate TDP-43 nucleocytoplasmic distribution. Furthermore, our observations raise the intriguing possibility that the cellular dynamics of other related RNA-associated proteins may be controlled in similar fashion.

Condensate formation plays a central role in RNP granule assembly and function [39] and our work suggests that it promotes TDP-43 nuclear localization, as seen by deleting and/or disrupting the CR in the C-terminus. This region also interacts with different RNA-binding proteins including hnRNPs A1, A2, A3, B1, and C [63]. Therefore, association with these hnRNPs may also contribute to RNP granule formation and nuclear retention, and this possibility requires further investigation. We also observe a significant decrease in nuclear localization in the presence of A326P, M337P, and the ALS-linked mutation M337V and a reduction in the size of TDP-43 complexes with the A326P mutation, similar to the effect of ΔCR. We predict that these single-site substitutions do not abolish TDP-43 association with the partner hnRNPs. On the other hand, the substitutions significantly disrupt TDP-43 phase separation, as seen in vitro and in cells [32,41]. Therefore, we posit that CR contributes to TDP-43 nuclear localization primarily through homotypic assembly and phase separation.

Collectively, our findings suggest the intriguing possibility that functional defects previously observed with oligomerization-deficient and other mutants/conditions affecting TDP-43 self-assembly may be at least partially caused by decreased nuclear localization. Since the structural characterization of TDP-43 NTD-mediated oligomerization [29,44], this interaction has been increasingly shown to play a central role in cellular functions. NTD-driven oligomerization is required for TDP-43 function in alternative splicing regulation [29,44], phase separation [10,44], autoregulation [40], and in preventing R-loop accumulation [14]. Here, we find that impaired oligomerization greatly reduces nuclear TDP-43 localization (**Fig 1C**), indicating that loss of function due to inhibition of NTD-mediated oligomerization may be caused by multiple mechanisms. These defects may include decreased self-assembly upon RNA target engagement, reduced RNP body formation, and decreased nuclear concentration.
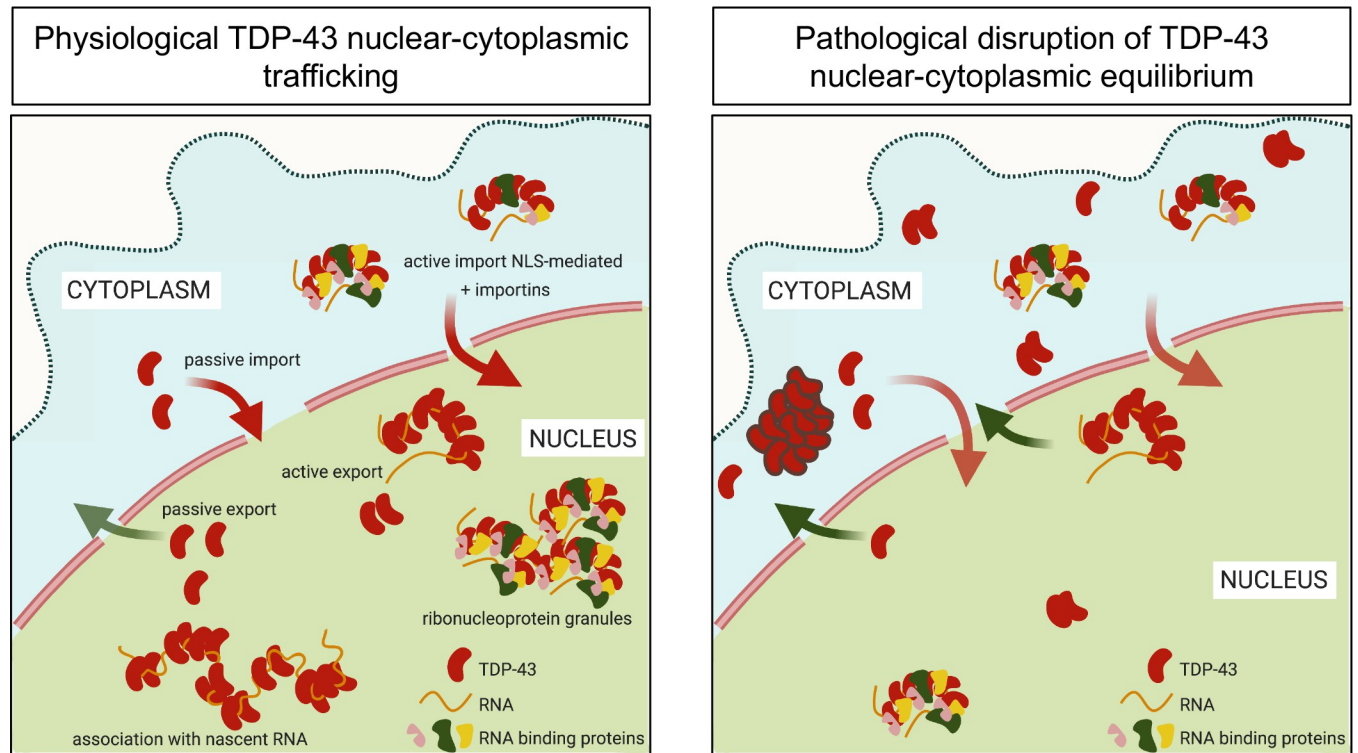
Fig 6. TDP-43 nuclear localization depends on the assembly of RNP complexes mediated via multivalent interactions. RNP TDP-43 complexes in the nucleus contribute to TDP-43 nuclear localization through the formation of higher-order macromolecular assemblies unable to passively diffuse to the cytoplasm. Under aberrant conditions, disruption of RNA binding or self-assembly increases levels of smaller TDP-43 species inducing greater cytoplasmic localization. Chronic defects in RNP assembly may increase TDP-43 misfolding and aggregation in the cytoplasm. RNP, ribonucleoprotein.

https://doi.org/10.1371/journal.pbio.3002527.g006

Importantly, our work suggests that TDP-43 nuclear efflux to the cytoplasm may be regulated by posttranslational modifications, mainly through phosphorylation at Ser48 in the NTD. We show that the phosphomimetic mutation S48E, which inhibits NTD-driven oligomerization [44], decreases nuclear TDP-43 localization by almost 50%. Thus, phosphorylation at Ser48 may normally tune TDP-43 nuclear-cytoplasmic distribution and aberrant activation of the phosphorylation pathways, which remain unknown, may contribute to increased cytoplasmic TDP-43 accumulation.

Together, our studies highlight multiple mechanisms that control TDP-43 RNP assembly and nuclear-cytoplasmic distribution through different types of interactions mediated by distinct TDP-43 domains, including binding to various RNA sequences with different affinities. This idea also implies that dysfunction of these regulatory factors may result in abnormal or pathological cytoplasmic TDP-43 accumulation. Therefore, these mechanisms may be targeted for therapeutic intervention to restore TDP-43 homeostasis and function.

Materials and methods

Chemicals were purchased from Sigma Aldrich unless otherwise specified.

Cloning, cell culture, and stable cell production

Generation of HEK293[HA-TDP-43] stable cell lines, expressing HA-tagged WT, E17R, S48A, S48E, M337V, and ΔCR constructs and stable cell lines was previously described [40]. Mutants A326P and M337P were generated by site-directed mutagenesis as previously described [10]

using the primers listed in S1 Table. Briefly, the HEK293-derived cells Flp-In T-Rex 293 Cell Line (Thermo Fisher Scientific) were stably transfected to express HA-TDP-43 upon induction with tetracycline (1 μg/ml). Cells were grown and maintained in DMEM (Dulbecco's Modified Eagle's Medium–High Glucose, Corning) supplemented with 10% FBS (fetal bovine serum) and incubated in a humid atmosphere at 37˚C and 5% CO_2. Expression of HA-tagged TDP-43 construct was induced at 30% confluence.

Cell fractionation

Stable cell lines cultured in 10 mm dishes (TPP) were induced with 1 μg/ml tetracycline for 72 h prior to harvesting and were pelleted through centrifugation at 300g for 5 min. Cell pellets were washed twice with PBS (phosphate-buffered saline) and gently resuspended in 2 ml of Lysis Buffer A (10 mM HEPES (pH 7.9), 1.5 mM $MgCl_2$, 10 mM KCl, 1 mM TCEP, protease inhibitor cocktail, 10 mM NaF, 1.5 mM orthovanadate, 10 mM β-glycerol phosphate). Resuspended samples were incubated for 5 min on ice and Dounce homogenized with 10 strokes (Pyrex, No 7727). Samples were pelleted at 200g for 5 min and supernatants were collected as cytoplasmatic fractions. The pellets were rinsed in 2 ml of PBS and pelleted at 200g for 5 min. The pellets were resuspended in 500 μl of PBS to obtain the nuclear fraction. All fractionation steps were carried out at 4˚C using cold buffers. Fractions were mixed with Laemmli buffer (0.2 M Tris (pH 6.8), 20% Glycerol, 10% SDS, 1.43 M β-mercaptoethanol, 0.05% bromophenol blue) and heated for 5 min at 95˚C. Equal volumes were resolved in standard 12% SDS-PAGE and immunoblotted against specified antibodies.

Heterokaryon assay

HEK293[HA-TDP-43] cells were grown on glass coverslips and heterokaryon assays were performed as previously described [20].

1,6-Hexanediol treatment

A total of 5% 1,6-hexanendiol was added to HEK293[HA-TDP-43] cells cultured at 80 to 90% confluency for 5 min prior to harvesting.

Size exclusion chromatography

HEK293[HA-TDP-43] cells were harvested at 90% to 100% confluence following 72 h of tetracycline induction. Cells were washed with PBS and resuspended in lysis buffer (25 mM Tris HCl (pH 7.5), 0.1 mM Na_3VO_4, 10 mM $MgCl_2$, protease inhibitor cocktail, 150 mM NaCl, 0.5% NP-40, 2 mM DTT, 5 mM β glycerophosphate) and processed using a Dounce homogenizer with 20 strokes (Pyrex, No 7727). Following centrifugation, soluble proteins were applied to the size exclusion gel filtration column (Superdex 200 Increase 10/300 GL, GE Healthcare), using an Akta P-920 Pump FPLC system (Amersham) and Running Buffer: 25 mM Tris-HCl (pH 7.5), 150 mM NaCl. Fractions were collected at 0.5 ml min^{-1}. The resulting dilution from input lysate was approximately 60-fold. Fractions were analyzed by standard SDS-PAGE followed by immunoblotting. The approximate molecular weight of each fraction was determined based on the elution volumes of thyoglobulin (670 KDa), γ globulin (158 KDa), ovalbumin (44 KDa), myoglobin (17 KDa), vitamin B12 (13.5 KDa), according to manufacturer's instructions.

High content analysis of RNA-dependent TDP-43 localization

HEK293[HA-TDP-43] cell lines (WT, F4L, E17R, and delta-CR) were plated on Ultimatrix-coated (1:100, R&D), 96-well optical plastic plates (Ibidi) to achieve approximately 75% confluence.

Doxycycline (1 µg/ml) was added to culture media at the time of plating, targeting 24 h of induction at the time of fixation. Transcriptional blockade was by NVP2 (250 nM, Tocris) or actinomycin D (1 µm) for 2 h. RNA oligonucleotides (IDT, see table) were transfected using Lipofectamine RNAiMax (Thermo Fisher) according to the manufacturer's instructions except that the lipofectamine amount was doubled based on initial optimization studies. Cells were fixed for analysis 5 h post-transfection. To determine the localization of HA-tagged TDP-43 and mutants, cells were fixed with 4% paraformaldehyde in PBS, permeabilized and blocked in 0.1% Tx-100 and 10% normal goat serum (Vector Labs), and immunostained with rabbit anti-HA (1:1,500, Cell Signaling Technologies) overnight at 4°C in 10% NGS/PBS. After 2 PBS rinses, Alexa Fluor-labeled secondary antibodies were added for 1 h at room temperature (1:1,000, Thermo). Cells were rinsed with PBS containing Hoechst 33342 and transferred to 50% glycerol/PBS for automated imaging and analysis using an ImageXpress Micro Confocal high content microscope with MetaXpress software (Molecular Devices) as described (Duan and colleagues). A minimum of 4 independent biological replicates was analyzed per experiment.

Confocal imaging

Glass coverslips were pre-coated with poly-D-lysine (0.1 mg/ml) for 10 min, then rinsed with PBS 3 times and left to dry under the tissue culture hood for at least 1 h. HEK293$^{HA-TDP-43}$ cells were plated on the pre-treated coverslips. After 24 h, cells were treated with Tet to induce HA-TDP-43 expression and fixed 48 h post-induction. Cells were fixed in 4% paraformaldehyde in PBS for 20 min, washed with PBS 3 times. Immunofluorescence was performed as previously described [61] using HA antibody and coilin antibody to label Cajal bodies. Imaging was performed with a Leica TCS SP8 confocal microscope with a 63× objective.

Supporting information

S1 Fig. Defects in TDP-43 self-assembly and RNA binding decrease nuclear localization.
(PDF)

S2 Fig. Inhibition of phase separation disrupts TDP-43 nuclear retention.
(PDF)

S3 Fig. Cellular distribution of WT and mutant TDP-43 as seen by microscopy.
(PDF)

S4 Fig. TDP-43 macromolecular complex distribution in total cell lysate.
(PDF)

S1 Table. List of DNA and RNA oligonucleotides used in our studies.
(PDF)

S1 Data. Supporting data.
(XLSX)

S1 Raw Images. Original immunoblot images for Figs 1B, 5A, S1B, S2A, S2B and S4.
(PDF)

Acknowledgments

Author Contributions

Conceptualization: Lindsey R. Hayes, Yuna M. Ayala.

Data curation: Erandika H. Hemamali, Lohany D. Mamede, Lindsey R. Hayes.

Formal analysis: Patricia M. dos Passos, Erandika H. Hemamali, Lindsey R. Hayes.

Funding acquisition: Lindsey R. Hayes, Yuna M. Ayala.

Investigation: Patricia M. dos Passos, Erandika H. Hemamali, Lohany D. Mamede, Lindsey R. Hayes.

Project administration: Yuna M. Ayala.

Supervision: Yuna M. Ayala.

Writing – original draft: Lindsey R. Hayes, Yuna M. Ayala.

Writing – review & editing: Patricia M. dos Passos, Erandika H. Hemamali, Lindsey R. Hayes, Yuna M. Ayala.

References

1. Neumann M, Sampathu DM, Kwong LK, Truax AC, Micsenyi MC, Chou TT, et al. Ubiquitinated TDP-43 in frontotemporal lobar degeneration and amyotrophic lateral sclerosis. Science. 2006; 314(5796):130–133. https://doi.org/10.1126/science.1134108 PMID: 17023659.

2. Arai T, Hasegawa M, Akiyama H, Ikeda K, Nonaka T, Mori H, et al. TDP-43 is a component of ubiquitin-positive tau-negative inclusions in frontotemporal lobar degeneration and amyotrophic lateral sclerosis. Biochem Biophys Res Commun. 2006; 351(3):602–611. https://doi.org/10.1016/j.bbrc.2006.10.093 PMID: 17084815.

3. Neumann M, Igaz LM, Kwong LK, Nakashima-Yasuda H, Kolb SJ, Dreyfuss G, et al. Absence of hetero-geneous nuclear ribonucleoproteins and survival motor neuron protein in TDP-43 positive inclusions in frontotemporal lobar degeneration. Acta Neuropathol. 2007; 113(5):543–8. Epub 2007/04/07. https://doi.org/10.1007/s00401-007-0221-x PMID: 17415574.

4. Nelson PT, Dickson DW, Trojanowski JQ, Jack CR, Boyle PA, Arfanakis K, et al. Limbic-predominant age-related TDP-43 encephalopathy (LATE): consensus working group report. Brain. 2019; 142 (6):1503–27. Epub 2019/05/01. https://doi.org/10.1093/brain/awz099 PMID: 31039256; PubMed Central PMCID: PMC6536849.

5. Coyne AN, Rothstein JD. Nuclear pore complexes—a doorway to neural injury in neurodegeneration. Nat Rev Neurol. 2022; 18(6):348–62. Epub 2022/04/30. https://doi.org/10.1038/s41582-022-00653-6 PMID: 35488039; PubMed Central PMCID: PMC10015220.

6. Winton MJ, Igaz LM, Wong MM, Kwong LK, Trojanowski JQ, Lee VM. Disturbance of Nuclear and Cyto-plasmic TAR DNA-binding Protein (TDP-43) Induces Disease-like Redistribution, Sequestration, and Aggregate Formation. J Biol Chem. 2008; 283(19):13302–13309. https://doi.org/10.1074/jbc.M800342200 PMID: 18305110.

7. Mann JR, Gleixner AM, Mauna JC, Gomes E, DeChellis-Marks MR, Needham PG, et al. RNA Binding Antagonizes Neurotoxic Phase Transitions of TDP-43. Neuron. 2019. Epub 2019/03/04. https://doi.org/10.1016/j.neuron.2019.01.048 PMID: 30826182.

8. Gasset-Rosa F, Lu S, Yu H, Chen C, Melamed Z, Guo L, et al. Cytoplasmic TDP-43 De-mixing Indepen-dent of Stress Granules Drives Inhibition of Nuclear Import, Loss of Nuclear TDP-43, and Cell Death. Neuron. 2019; 102(2):339–57 e7. Epub 2019/03/12. https://doi.org/10.1016/j.neuron.2019.02.038 PMID: 30853299.

9. Maharana S, Wang J, Papadopoulos DK, Richter D, Pozniakovsky A, Poser I, et al. RNA buffers the phase separation behavior of prion-like RNA binding proteins. Science. 2018; 360(6391):918–21. Epub 2018/04/14. https://doi.org/10.1126/science.aar7366 PMID: 29650702; PubMed Central PMCID: PMC6091854.

10. Grese ZR, Bastos AC, Mamede LD, French RL, Miller TM, Ayala YM. Specific RNA interactions pro-mote TDP-43 multivalent phase separation and maintain liquid properties. EMBO Rep. 2021; 22(12): e53632. Epub 2021/11/18. https://doi.org/10.15252/embr.202153632 PMID: 34787357; PubMed Central PMCID: PMC8647020.

11. Tollervey JR, Curk T, Rogelj B, Briese M, Cereda M, Kayikci M, et al. Characterizing the RNA targets and position-dependent splicing regulation by TDP-43. Nat Neurosci. 2011; 14(4):452–8. Epub 2011/03/02. https://doi.org/10.1038/nn.2778 PMID: 21358640; PubMed Central PMCID: PMC3108889.

12. Polymenidou M, Lagier-Tourenne C, Hutt KR, Huelga SC, Moran J, Liang TY, et al. Long pre-mRNA depletion and RNA missplicing contribute to neuronal vulnerability from loss of TDP-43. Nat Neurosci. 2011; 14(4):459–68. Epub 2011/03/02. https://doi.org/10.1038/nn.2779 PMID: 21358643; PubMed Central PMCID: PMC3094729.

13. Rot G, Wang Z, Huppertz I, Modic M, Lence T, Hallegger M, et al. High-Resolution RNA Maps Suggest Common Principles of Splicing and Polyadenylation Regulation by TDP-43. Cell Rep. 2017; 19 (5):1056–67. Epub 2017/05/04. https://doi.org/10.1016/j.celrep.2017.04.028 PMID: 28467899; PubMed Central PMCID: PMC5437728.

14. Wood M, Quinet A, Lin YL, Davis AA, Pasero P, Ayala YM, et al. TDP-43 dysfunction results in R-loop accumulation and DNA replication defects. J Cell Sci. 2020; 133(20). Epub 2020/09/30. https://doi.org/10.1242/jcs.244129 PMID: 32989039; PubMed Central PMCID: PMC7648616.

15. Liu EY, Russ J, Cali CP, Phan JM, Amlie-Wolf A, Lee EB. Loss of Nuclear TDP-43 Is Associated with Decondensation of LINE Retrotransposons. Cell Rep. 2019; 27(5):1409–21 e6. Epub 2019/05/03. https://doi.org/10.1016/j.celrep.2019.04.003 PMID: 31042469; PubMed Central PMCID: PMC6508629.

16. Ling JP, Pletnikova O, Troncoso JC, Wong PC. TDP-43 repression of nonconserved cryptic exons is compromised in ALS-FTD. Science. 2015; 349(6248):650–5. Epub 2015/08/08. https://doi.org/10.1126/science.aab0983 PMID: 26250685; PubMed Central PMCID: PMC4825810.

17. Melamed Z, Lopez-Erauskin J, Baughn MW, Zhang O, Drenner K, Sun Y, et al. Premature polyadenylation-mediated loss of stathmin-2 is a hallmark of TDP-43-dependent neurodegeneration. Nat Neurosci. 2019; 22(2):180–90. Epub 2019/01/16. https://doi.org/10.1038/s41593-018-0293-z PMID: 30643298; PubMed Central PMCID: PMC6348009.

18. Brown AL, Wilkins OG, Keuss MJ, Hill SE, Zanovello M, Lee WC, et al. TDP-43 loss and ALS-risk SNPs drive mis-splicing and depletion of UNC13A. Nature. 2022; 603(7899):131–7. Epub 2022/02/25. https://doi.org/10.1038/s41586-022-04436-3 PMID: 35197628; PubMed Central PMCID: PMC8891020 described in this work has been protected in the patent PCT/EP2021/084908 and UK patent 2117758.9 (patent applicant, UCL Business Ltd and NIH; status pending), in which A.-L.B., O.G.W., M.J.K., S.E. H., M.E.W. and P.F. are named as inventors. The other authors declare no competing interests.

19. Ma XR, Prudencio M, Koike Y, Vatsavayai SC, Kim G, Harbinski F, et al. TDP-43 represses cryptic exon inclusion in the FTD-ALS gene UNC13A. Nature. 2022; 603(7899):124–30. Epub 2022/02/25. https://doi.org/10.1038/s41586-022-04424-7 PMID: 35197626; PubMed Central PMCID: PMC8891019 consultant for Maze Therapeutics. M.P. and L.P. serve as consultants for Target ALS. F.H., B.B.C., D. W.W., K.K., G. Miller, S. Mekhoubad, N.S. and E.G. are employees of Maze Therapeutics, which has filed a patent (63/171,522) on methods to modulate splicing of UNC13A.

20. Ayala YM, Zago P, D'Ambrogio A, Xu YF, Petrucelli L, Buratti E, et al. Structural determinants of the cellular localization and shuttling of TDP-43. J Cell Sci. 2008; 121(Pt 22):3778–85. Epub 2008/10/30. https://doi.org/10.1242/jcs.038950 PMID: 18957508.

21. Nishimura AL, Zupunski V, Troakes C, Kathe C, Fratta P, Howell M, et al. Nuclear import impairment causes cytoplasmic trans-activation response DNA-binding protein accumulation and is associated with frontotemporal lobar degeneration. Brain. 2010; 133(Pt 6):1763–71. Epub 2010/05/18. https://doi.org/10.1093/brain/awq111 PMID: 20472655.

22. Timney BL, Raveh B, Mironska R, Trivedi JM, Kim SJ, Russel D, et al. Simple rules for passive diffusion through the nuclear pore complex. J Cell Biol. 2016; 215(1):57–76. Epub 2016/10/05. https://doi.org/10.1083/jcb.201601004 PMID: 27697925; PubMed Central PMCID: PMC5057280.

23. Ederle H, Funk C, Abou-Ajram C, Hutten S, Funk EBE, Kehlenbach RH, et al. Nuclear egress of TDP-43 and FUS occurs independently of Exportin-1/CRM1. Sci Rep. 2018; 8(1):7084. Epub 2018/05/08. https://doi.org/10.1038/s41598-018-25007-5 PMID: 29728564; PubMed Central PMCID: PMC5935713.

24. Pinarbasi ES, Cagatay T, Fung HYJ, Li YC, Chook YM, Thomas PJ. Active nuclear import and passive nuclear export are the primary determinants of TDP-43 localization. Sci Rep. 2018; 8(1):7083. Epub 2018/05/08. https://doi.org/10.1038/s41598-018-25008-4 PMID: 29728608; PubMed Central PMCID: PMC5935693.

25. Archbold HC, Jackson KL, Arora A, Weskamp K, Tank EM, Li X, et al. TDP43 nuclear export and neurodegeneration in models of amyotrophic lateral sclerosis and frontotemporal dementia. Sci Rep. 2018; 8 (1):4606. Epub 2018/03/17. https://doi.org/10.1038/s41598-018-22858-w PMID: 29545601; PubMed Central PMCID: PMC5854632.

26. Duan L, Zaepfel BL, Aksenova V, Dasso M, Rothstein JD, Kalab P, et al. Nuclear RNA binding regulates TDP-43 nuclear localization and passive nuclear export. Cell Rep. 2022; 40(3):111106. Epub 2022/07/

21. https://doi.org/10.1016/j.celrep.2022.111106 PMID: 35858577; PubMed Central PMCID: PMC9345261.

27. Mohr D, Frey S, Fischer T, Guttler T, Gorlich D. Characterisation of the passive permeability barrier of nuclear pore complexes. EMBO J. 2009; 28(17):2541–53. Epub 2009/08/15. https://doi.org/10.1038/emboj.2009.200 PMID: 19680228; PubMed Central PMCID: PMC2728435.

28. Mompean M, Romano V, Pantoja-Uceda D, Stuani C, Baralle FE, Buratti E, et al. The TDP-43 N-terminal domain structure at high resolution. FEBS J. 2016; 283(7):1242–60. Epub 2016/01/13. https://doi.org/10.1111/febs.13651 PMID: 26756435.

29. Afroz T, Hock EM, Ernst P, Foglieni C, Jambeau M, Gilhespy LAB, et al. Functional and dynamic polymerization of the ALS-linked protein TDP-43 antagonizes its pathologic aggregation. Nat Commun. 2017; 8(1):45. Epub 2017/07/01. https://doi.org/10.1038/s41467-017-00062-0 PMID: 28663553; PubMed Central PMCID: PMC5491494.

30. Ayala YM, Pantano S, D'Ambrogio A, Buratti E, Brindisi A, Marchetti C, et al. Human, Drosophila, and C.elegans TDP43: nucleic acid binding properties and splicing regulatory function. J Mol Biol. 2005; 348 (3):575–88. Epub 2005/04/14. https://doi.org/10.1016/j.jmb.2005.02.038 PMID: 15826655.

31. Lukavsky PJ, Daujotyte D, Tollervey JR, Ule J, Stuani C, Buratti E, et al. Molecular basis of UG-rich RNA recognition by the human splicing factor TDP-43. Nat Struct Mol Biol. 2013. Epub 2013/11/19. https://doi.org/10.1038/nsmb.2698 PMID: 24240615.

32. Conicella AE, Zerze GH, Mittal J, Fawzi NL. ALS Mutations Disrupt Phase Separation Mediated by alpha-Helical Structure in the TDP-43 Low-Complexity C-Terminal Domain. Structure. 2016; 24 (9):1537–49. Epub 2016/08/23. https://doi.org/10.1016/j.str.2016.07.007 PMID: 27545621; PubMed Central PMCID: PMC5014597.

33. Schmidt HB, Rohatgi R. In Vivo Formation of Vacuolated Multi-phase Compartments Lacking Membranes. Cell Rep. 2016; 16(5):1228–36. Epub 2016/07/28. https://doi.org/10.1016/j.celrep.2016.06.088 PMID: 27452472; PubMed Central PMCID: PMC4972689.

34. Lim L, Wei Y, Lu Y, Song J. ALS-Causing Mutations Significantly Perturb the Self-Assembly and Interaction with Nucleic Acid of the Intrinsically Disordered Prion-Like Domain of TDP-43. PLoS Biol. 2016; 14(1):e1002338. Epub 2016/01/07. https://doi.org/10.1371/journal.pbio.1002338 PMID: 26735904; PubMed Central PMCID: PMC4703307.

35. Brangwynne CP, Eckmann CR, Courson DS, Rybarska A, Hoege C, Gharakhani J, et al. Germline P granules are liquid droplets that localize by controlled dissolution/condensation. Science. 2009; 324 (5935):1729–32. Epub 2009/05/23. https://doi.org/10.1126/science.1172046 PMID: 19460965.

36. Strom AR, Brangwynne CP. The liquid nucleome—phase transitions in the nucleus at a glance. J Cell Sci. 2019; 132(22). Epub 2019/11/23. https://doi.org/10.1242/jcs.235093 PMID: 31754043; PubMed Central PMCID: PMC6899023.

37. Tsuiji H, Iguchi Y, Furuya A, Kataoka A, Hatsuta H, Atsuta N, et al. Spliceosome integrity is defective in the motor neuron diseases ALS and SMA. EMBO Mol Med. 2013; 5(2):221–34. Epub 2012/12/21. https://doi.org/10.1002/emmm.201202303 PMID: 23255347; PubMed Central PMCID: PMC3569639.

38. Colombrita C, Zennaro E, Fallini C, Weber M, Sommacal A, Buratti E, et al. TDP-43 is recruited to stress granules in conditions of oxidative insult. J Neurochem. 2009; 111(4):1051–61. Epub 2009/09/22. https://doi.org/10.1111/j.1471-4159.2009.06383.x PMID: 19765185.

39. Shin Y, Brangwynne CP. Liquid phase condensation in cell physiology and disease. Science. 2017;357 (6357). Epub 2017/09/25. https://doi.org/10.1126/science.aaf4382 PMID: 28935776.

40. Koehler LC, Grese ZR, Bastos ACS, Mamede LD, Heyduk T, Ayala YM. TDP-43 Oligomerization and Phase Separation Properties Are Necessary for Autoregulation. Front Neurosci. 2022;16. https://doi.org/10.3389/fnins.2022.818655 PMID: 35495061

41. Hallegger M, Chakrabarti AM, Lee FCY, Lee BL, Amalietti AG, Odeh HM, et al. TDP-43 condensation properties specify its RNA-binding and regulatory repertoire. Cell. 2021; 184(18):4680–96 e22. Epub 2021/08/12. https://doi.org/10.1016/j.cell.2021.07.018 PMID: 34380047.

42. Ayala YM, De Conti L, Avendano-Vazquez SE, Dhir A, Romano M, D'Ambrogio A, et al. TDP-43 regulates its mRNA levels through a negative feedback loop. EMBO J. 2011; 30(2):277–88. Epub 2010/12/07. https://doi.org/10.1038/emboj.2010.310 PMID: 21131904; PubMed Central PMCID: PMC3025456.

43. Buratti E, Baralle FE. Characterization and functional implications of the RNA binding properties of nuclear factor TDP-43, a novel splicing regulator of CFTR exon 9. J Biol Chem. 2001; 276(39):36337–36343. https://doi.org/10.1074/jbc.M104236200 PMID: 11470789.

44. Wang A, Conicella AE, Schmidt HB, Martin EW, Rhoads SN, Reeb AN, et al. A single N-terminal phosphomimic disrupts TDP-43 polymerization, phase separation, and RNA splicing. EMBO J. 2018. Epub 2018/02/14. https://doi.org/10.15252/embj.201797452 PMID: 29438978.

45. Rigbolt KT, Prokhorova TA, Akimov V, Henningsen J, Johansen PT, Kratchmarova I, et al. System-wide temporal characterization of the proteome and phosphoproteome of human embryonic stem cell differentiation. Sci Signal. 2011; 4(164):rs3. Epub 2011/03/17. https://doi.org/10.1126/scisignal.2001570 PMID: 21406692.

46. Hornbeck PV, Zhang B, Murray B, Kornhauser JM, Latham V, Skrzypek E. PhosphoSitePlus, 2014: mutations, PTMs and recalibrations. Nucleic Acids Res. 2015; 43(Database issue):D512–20. Epub 2014/12/18. https://doi.org/10.1093/nar/gku1267 PMID: 25514926; PubMed Central PMCID: PMC4383998.

47. Olson CM, Jiang B, Erb MA, Liang Y, Doctor ZM, Zhang Z, et al. Pharmacological perturbation of CDK9 using selective CDK9 inhibition or degradation. Nat Chem Biol. 2018; 14(2):163–70. Epub 2017/12/19. https://doi.org/10.1038/nchembio.2538 PMID: 29251720; PubMed Central PMCID: PMC5912898.

48. Bennett CF, Swayze EE. RNA targeting therapeutics: molecular mechanisms of antisense oligonucleo-tides as a therapeutic platform. Annu Rev Pharmacol Toxicol. 2010; 50:259–93. Epub 2010/01/09. https://doi.org/10.1146/annurev.pharmtox.010909.105654 PMID: 20055705.

49. Molliex A, Temirov J, Lee J, Coughlin M, Kanagaraj AP, Kim HJ, et al. Phase separation by low complexity domains promotes stress granule assembly and drives pathological fibrillization. Cell. 2015; 163 (1):123–33. Epub 2015/09/26. https://doi.org/10.1016/j.cell.2015.09.015 PMID: 26406374; PubMed Central PMCID: PMC5149108.

50. Murakami T, Qamar S, Lin JQ, Schierle GS, Rees E, Miyashita A, et al. ALS/FTD Mutation-Induced Phase Transition of FUS Liquid Droplets and Reversible Hydrogels into Irreversible Hydrogels Impairs RNP Granule Function. Neuron. 2015; 88(4):678–90. Epub 2015/11/04. https://doi.org/10.1016/j.neuron.2015.10.030 PMID: 26526393; PubMed Central PMCID: PMC4660210.

51. Patel A, Lee HO, Jawerth L, Maharana S, Jahnel M, Hein MY, et al. A Liquid-to-Solid Phase Transition of the ALS Protein FUS Accelerated by Disease Mutation. Cell. 2015; 162(5):1066–77. Epub 2015/09/01. https://doi.org/10.1016/j.cell.2015.07.047 PMID: 26317470.

52. Mackenzie IR, Nicholson AM, Sarkar M, Messing J, Purice MD, Pottier C, et al. TIA1 Mutations in Amyotrophic Lateral Sclerosis and Frontotemporal Dementia Promote Phase Separation and Alter Stress Granule Dynamics. Neuron. 2017; 95(4):808–16 e9. Epub 2017/08/18. https://doi.org/10.1016/j.neuron.2017.07.025 PMID: 28817800; PubMed Central PMCID: PMC5576574.

53. Kroschwald S, Maharana S, Alberti S. Hexanediol: a chemical probe to investigate the material properties of membrane-less compartments. Matters. 2017:2297–8240. https://doi.org/10.19185/matters.201702000010

54. Schmidt HB, Barreau A, Rohatgi R. Phase separation-deficient TDP43 remains functional in splicing. Nat Commun. 2019; 10(1):4890. Epub 2019/10/28. https://doi.org/10.1038/s41467-019-12740-2 PMID: 31653829; PubMed Central PMCID: PMC6814767.

55. Ribbeck K, Gorlich D. The permeability barrier of nuclear pore complexes appears to operate via hydrophobic exclusion. EMBO J. 2002; 21(11):2664–71. Epub 2002/05/29. https://doi.org/10.1093/emboj/21.11.2664 PMID: 12032079; PubMed Central PMCID: PMC126029.

56. Conicella AE, Dignon GL, Zerze GH, Schmidt HB, D'Ordine AM, Kim YC, et al. TDP-43 alpha-helical structure tunes liquid-liquid phase separation and function. Proc Natl Acad Sci U S A. 2020; 117 (11):5883–94. Epub 2020/03/07. https://doi.org/10.1073/pnas.1912055117 PMID: 32132204; PubMed Central PMCID: PMC7084079.

57. Guo W, Chen Y, Zhou X, Kar A, Ray P, Chen X, et al. An ALS-associated mutation affecting TDP-43 enhances protein aggregation, fibril formation and neurotoxicity. Nat Struct Mol Biol. 2011; 18(7):822–30. Epub 2011/06/15. https://doi.org/10.1038/nsmb.2053 PMID: 21666678; PubMed Central PMCID: PMC3357956.

58. Mallam AL, Sae-Lee W, Schaub JM, Tu F, Battenhouse A, Jang YJ, et al. Systematic Discovery of Endogenous Human Ribonucleoprotein Complexes. Cell Rep. 2019; 29(5):1351–68 e5. Epub 2019/10/31. https://doi.org/10.1016/j.celrep.2019.09.060 PMID: 31665645; PubMed Central PMCID: PMC6873818.

59. Bentmann E, Neumann M, Tahirovic S, Rodde R, Dormann D, Haass C. Requirements for stress granule recruitment of fused in sarcoma (FUS) and TAR DNA-binding protein of 43 kDa (TDP-43). J Biol Chem. 2012; 287(27):23079–94. Epub 2012/05/09. https://doi.org/10.1074/jbc.M111.328757 PMID: 22563080; PubMed Central PMCID: PMC3391091.

60. Schmidt HB, Rohatgi R. High-throughput Flow Cytometry Assay to Investigate TDP43 Splicing Function. Bio Protoc. 2020; 10(8):e3594. Epub 2021/03/05. https://doi.org/10.21769/BioProtoc.3594 PMID: 33659560; PubMed Central PMCID: PMC7842676.

61. French RL, Grese ZR, Aligireddy H, Dhavale DD, Reeb AN, Kedia N, et al. Detection of TAR DNA-binding protein 43 (TDP-43) oligomers as initial intermediate species during aggregate formation. J Biol

Chem. 2019; 294(17):6696–709. Epub 2019/03/03. https://doi.org/10.1074/jbc.RA118.005889 PMID: 30824544; PubMed Central PMCID: PMC6497947.

62. Perez-Berlanga M, Wiersma VI, Zbinden A, De Vos L, Wagner U, Foglieni C, et al. Loss of TDP-43 olig-omerization or RNA binding elicits distinct aggregation patterns. EMBO J. 2023:e111719. Epub 2023/07/11. https://doi.org/10.15252/embj.2022111719 PMID: 37431963.

63. D'Ambrogio A, Buratti E, Stuani C, Guarnaccia C, Romano M, Ayala YM, et al. Functional mapping of the interaction between TDP-43 and hnRNP A2 in vivo. Nucleic Acids Res. 2009; 37(12):4116–26. Epub 2009/05/12. https://doi.org/10.1093/nar/gkp342 PMID: 19429692; PubMed Central PMCID: PMC2709582.